Orissa Journal of Physics
ISSN 0974-8202

Vol. 22, No.1
February 2015
pp. 149-160

# Nanotechnology and Photovoltaics

R M PUJAHARI[1, 3] and M C ADHIKARY[2]
Echelon Institute of Technology, Faridabad, India
Dept. of Applied Physics and Ballistics, F M University, Balasore, India
[3]Corresponding author, E-mail: rpujahari@gmail.com

*Received : 12.11.2014 ; Accepted : 15.1.2015*

**Abstract:** Highly crystalline dispersive NiO nanocrystals have been synthesised with a diameter of 2.5±0.5 nm. It is possible to synthesise nanocrystals without heating which has not been previously reported. Very large rod-shaped particles were selectively synthesised using increased reflux time and reactant concentration, which can be separated from the smaller particles using filtration or sedimentation. Permittivity and conductivity measurements of nanocrystal solutions provide evidence of rotational and translational degrees of freedom.

**Keywords** - Metal-oxide Nanocrystals; TEM image of NiO rods; anodisation; electropolishing

## 1. Introduction

Authoritative projections place solar power as a significant, and quite possibly the dominant, post-fossil-fuel power source [1]. This is on account of the abundance and ubiquity of sunlight. In fact, a 15% efficient solar power station of surface area equal to 15% of India would generate sufficient electricity and fuel for the entire global requirements of electricity, heating, and transport. While crystalline silicon has been the mainstay photovoltaic (PV) cell material for the past 30 years, reaching efficiencies of 20%, the requirement for high purity materials has kept the production costs stubbornly high. High production costs mean PV is currently not cost competitive with other sources, being approximately 4 times more expensive than wind or nuclear, and 8 times more expensive than coal [2]. The energy intensive production of silicon PV means lifecycle greenhouse gas emissions are greater than wind or nuclear. Despite the recent boom in PV installation, less than 0.1% of electricity is currently generated from PV. For these reasons, it looks unlikely that crystalline silicon PV will ever become our dominant power generation technology.

A massive worldwide research effort is underway to develop new materials, new cell architectures, and new production routes for a low-cost high-efficiency PV cell. One option is to boost the efficiency of inherently cheaper, innovative, and disruptive designs such as polymer (organic) or metal oxide PV by incorporating nanostructure [3]. This is primarily because nanomaterials offer increased optical absorption, the ability to tune their optical properties through size and shape, and often cheaper production routes aided by self assembly.

This paper focuses on semiconductor nanocrystals which are single-domain crystals of nanometre dimensions [4]. Of particular importance is the quantum size effect because this allows the absorption of the nanocrystal to be tuned to maximise conversion of the solar spectrum. When the size of the nanocrystal approaches the exciton Bohr radius, the effective bandgap increases to

$$E_{g-eff} = E_{g-bulk} + \frac{\pi^2 \hbar^2}{2m^* r^2} \quad (1)$$

where r is the nanocrystal radius and $m^*$ is the exciton effective mass which is a material property. This is observed as a shift in the absorption edge and the emission peak to shorter wavelengths which is commonly referred as a blue- or hypsochromic shift. The recent observation of multiple exciton generation (MEG) in nanocrystals, where each photon generates more than one electron, opens a further exciting possibility of low-cost nanocrystal-based PV cells with an impressive theoretical efficiency of 44% [5,6]. This is because MEG enables the efficient conversion of more than one part of the solar spectrum. Subsequent sections in this paper briefly consider the central fields of nanocrystal research: synthesis, characterisation, assembly, and application.

*Metal oxide nanocrystals*

Metal-oxide nanocrystals are usually wide-bandgap p-type semiconductors, although there are notable exceptions. Metal-oxides often consist of abundant elements of low-toxicity, and there exist low-cost nanocrystal synthesis routes, making them an attractive choice for PV applications such as the light conversion element, conductive transparent oxides, and electrodes in dye-sensitised cells. Other applications include photocatalysis, sensors, magnetic resonance imaging, targeted drug delivery, and solid oxide fuel cells. Table 1 lists some relevant properties of the metal oxides considered here.

**Table 1.** Properties of metal oxides.

| | bandgap | type | structure |
|---|---|---|---|
| ZnO | 3.4 eV direct | n | ZB |
| NiO | 3.6 eV direct | p | NaCl |
| $Cu_2O$ | 1.2 eV direct | p | Cubic |
| $Ag_2O$ | 1.4 eV direct | p | Cubic |

$Cu_2O$ and $Ag_2O$ have appropriate bandgaps for solar energy conversion, although control of nonstoichiometry is a problem because Cu and Ag are stable in multiple oxidation states. ZnO and NiO form a complementary pair with similar bandgaps and the possibility of a nanoscale p-n heterojunction as part of a tandem PV cell converting the UV part of the spectrum.

*Nanocrystal solution synthesis*

Metal oxide nanocrystals are synthesized by reflux of alcohol solutions of hydrated metal acetate under ambient conditions [7], following a method similar to that used by Wu et al. for ZnO [8,9]. Chemical and physical properties, including the configuration of deposited nanocrystals, are measured using transmission electron microscopy (TEM), energy-dispersive x-ray spectroscopy (EDX), selected area electron diffraction (SAED) and high angle annular dark field HAADF imaging. Optical properties are measured using spectroflorometry, photoluminescence, and a novel nanocrystal PV device which is discussed in section 5.0.

Nickel oxide is of particular interest due to a wide range of beneficial properties such as catalytic behaviour, anomalous electronic and magnetic properties [10-15]. A tight size distribution is crucial for practical applications because the optical, electrical, and chemical properties are sensitive to the nanocrystal size.

## 2. Experimental

Hydrated metal acetate was dissolved in methanol in the molar ratio of 0.03:4.00 and refluxed for 6 hours under ambient conditions, at a temperature of 67°C (the boiling point of the solution) and vigorous stirring. The above ratio was the starting point from which the concentration of the metal ions was varied by adding more metal acetate at various times during the reflux. In addition to this the reflux times were also varied. Cooling to room temperature (23°C) the organic capping agent 3-aminopropyltrimethoxysilane (AM),

$H_2N(CH_2)_3Si(OCH_3)_3$, is added to different samples at different times. A similar reflux hydrolysis method has been reported to produce CuO nanocrystals [16].

*Experimental Results*

Capped NiO nanocrystals were synthesised using a 6 hour reflux and a 0.03:4.00 molar ratio of NiAc:methanol. TEM, EDX and SAED analysis confirm the successful synthesis of highly dispersive spherical NiO nanocrystals. It can be seen from Fig. 1 that the NiO nanocrystals produced have a tight size distribution with an average particle diameter of 2.5±0.5 nm.

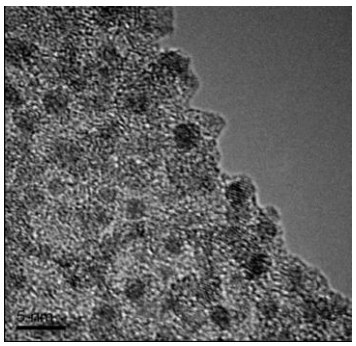

**Fig. 1.** TEM image of NiO nanocrystals capped with AM. The crystalline structure of the nanocrystals is evident.

**Table 2.** Experimental and tabulated lattice spacing from SEAD.

| Ring | d (Å) exp. | d (Å) tab. |
|---|---|---|
| 1 | 2.471 | 2.412 |
| 2 | 2.072 | 2.088 |
| 3 | 1.476 | 1.377 |

Nanocrystals were also synthesised without using the capping agent. Figure 2 shows the SAED pattern and table 2 presents the experimental and consistent NiO tabulated lattice spacings. The uncapped nanocrystals follow the same size distribution as the capped nanocrystals. Both capped and uncapped nanocrystals are highly crystalline.

**Fig. 2:** SAED pattern of uncapped NiO nanocrystals.

Figure 3 shows a TEM image of an eight hour reflux. The NiO particles produced here are significantly larger and elongated rod like particles. Smaller circular nanocrystals may still be present in the solution, but they were not present in this TEM sample. Synthesis was also performed using an increased concentration of nickel acetate. However, as shown in figure 4, some larger micron-sized particles were obtained. These particles show signs of agglomeration, and were readily separated using sedimentation.

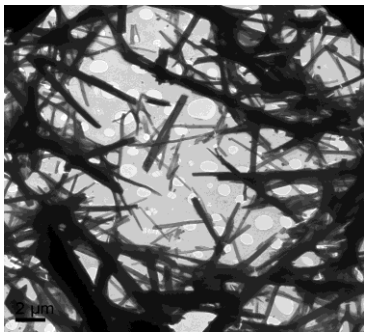


**Fig. 3:** TEM image of NiO rods produced after an 8 hour reflux.

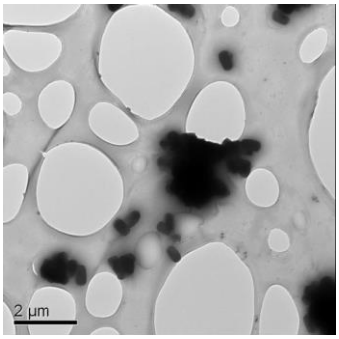


**Fig. 4:** TEM image of NiO micron sized particles produced from a 6 hour reflux but adding nickel acetate at various times during the reflux.

Figure 5 shows a typical energy dispersive x-ray (EDX) spectra of capped NiO nanocrystals to help confirm the elemental composition. In addition to Ni and O, Si is present in the capping agent and Cu is present in the TEM grid.

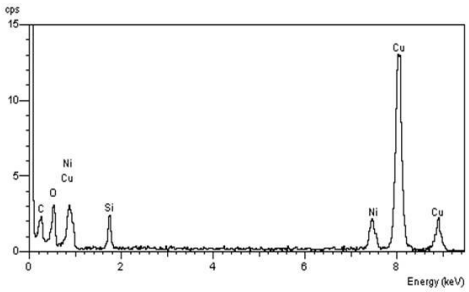


**Fig. 5.** EDX spectra of capped NiO nanocrystals.

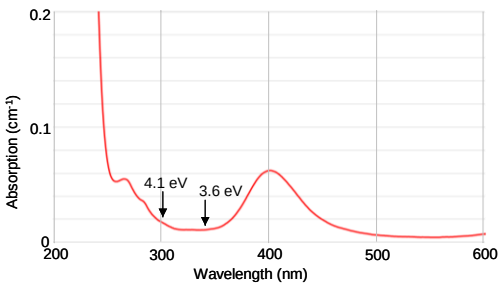


**Fig. 6.** Absorption spectra of capped NiO nanocrystals suspended in methanol.

**Nanocrystal characterisation**

Transmission electron microscopy with in-situ techniques such as SAED and EDX is arguably the most informative instrument with which to investigate nanocrystal structural, physical, and some electronic properties. Disadvantages include high cost and low throughput. Other common nanocrystal characterisation techniques include absorption and emission spectroscopy, x-ray diffraction, and dynamic light scattering.

***Absorption spectroscopy***

Absorption and emission spectroscopies can identify the effective bandgap which is related to the nanocrystal size through equation 1. However, this relationship does require an accurate knowledge of the bulk bandgap and the exciton effective mass. Multiple absorption edges or multiple emission peaks provide a rich source of information about the relative probability of absorption or recombination between quantum states, which is determined by composition, shape, and size. Figure 6 shows the absorption spectra for capped NiO nanocrystals suspended in methanol using a methanol reference.

***Permittivity and conductivity***

The potential of permittivity and conductivity as measurements of nanocrystal size, shape, and composition are evaluated. Permittivity, or dielectric constant, is mathematically related to polarizability, meaning the ability of a material to screen an external electric field.

In a typical experiment nanocrystals are suspended in methanol in a quartz cell with two gold ball electrodes separated by 240 μm. A variable-frequency signal generator applies a small AC voltage to one electrode, and the in-phase and out-of-phase AC current is measured from the second electrode using a lock-in amplifier. The set up also allows a DC bias to be applied to the source electrode and for the sample to be illuminated with UV light. Table 3 provides experimental measurements made at a low frequency.

| Material | $\varepsilon_r$ |
|---|---|
| ZnO bulk | 2 |
| Methanol | 81 |
| ZnO nanocrystals uncapped | 562 |
| ZnO nanocrystals capped | 1172 |

**Table 3.** Relative permittivity measured at 794 Hz.

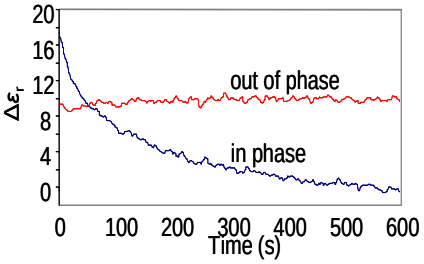


**Figure 7.** Change in relative permittivity under a DC bias for ZnO nanocrystals.

The massively enhanced permittivity of ZnO nanocrystals compared to bulk ZnO is caused by rotational or translational degrees of freedom which are not possible in bulk material. The in-phase signal, which is proportional to permittivity, decays with an approximate time constant of 105 s (this is much longer than any of the instrumental time constants).

**Nanocrystal assembly**

Nanocrystals suspended in solution require a further processing step to transfer them onto a substrate for all PV applications. The nanocrystals are required to arrange themselves into a close packed layer, driven by energy minimization, in a process known as self assembly. Various methods are available including: dip coating, the Langmuir-Blodgett method [19], spin coating, electrophoretic deposition [18], chemical bonding, and solvent evaporation.

***Chemical bonding***

The atomic force microscope (AFM) image in figure 8 shows individual CdSe nanocrystals attached to a Si substrate. This was achieved by soaking the clean Si substrate in a solution of capped CdSe nanocrystals, toluene, and MPS for 12 hours. The MPS behaves as a linker molecule to provide a strong chemical bond between Si and capped CdSe. The bond is strong so the nanocrystals do not have the opportunity to self assemble.

***Solvent evaporation***

The AFM image in figure 9 shows a monolayer of CdSe nanocrystals on a Si substrate. This was achieved by placing a drop of nanocrystal solution on the sample surface. The solvent slowly evaporates, and the nanocrystals self assemble into a monolayer.

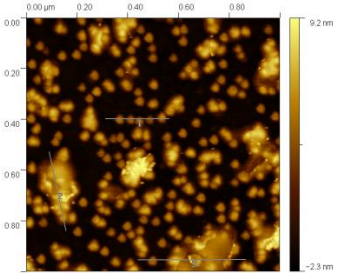


**Fig. 8.** AFM image of CdSe on Si deposited using chemical bonding.

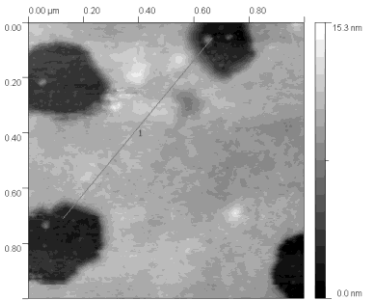


**Fig. 9.** AFM image of CdSe nanocrystals on Si substrate.

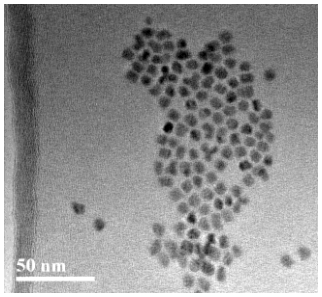


**Figure 10.** TEM image of CdSe nanocrystals on carbon grid.

Figure 10 shows a TEM image of CdSe nanocrystals deposited by solvent evaporation, again showing a self assembled hexagonal packing.

**Nanocrystal applications**

Nanocrystals have several potential applications in PV. One of the most appealing applications is to incorporate nanocrystals into existing PV designs.

***Nanocrystal solar cell***

A typical nanocrystal PV cell based on a novel hot-electron design [20-22] has been developed. The device structure is: titanium (substrate), titanium-dioxide layer, noble metal layer, photoreceptor layer. The photoreceptor can be either a photoactive dye or a nanocrystal monolayer. Titanium and titanium oxides are also receiving increased attention as substrate materials in other PV and photocatalysis designs primarily because of their photoactive properties, appropriate band structure, and chemical stability [23, 24].

***Experimental Method***

The two-stage process presented here separates control of microstructure formation from the electropolishing mechanism to provide a well controlled microstructure that is also smooth on the sub-micron scale. In stage one, titanium anodization create a surface oxide of thickness up to 50 nm (figure 11a). Dislocations and porosity are unavoidable in the oxide layer although their surface density and structure can be controlled by the choice of electrolyte and current [26-28]. In stage two, low-hazard alcoholic-electrolyte electropolishing removes titanium from beneath the oxide to etch the microstructure [29] (figure 11b). It is likely that the dislocations initially provide chemical channels for the electrolyte to etch cavities underneath the oxide layer. With further electropolishing the remaining oxide is removed and sharp protrusions are smoothed (figure 11c).

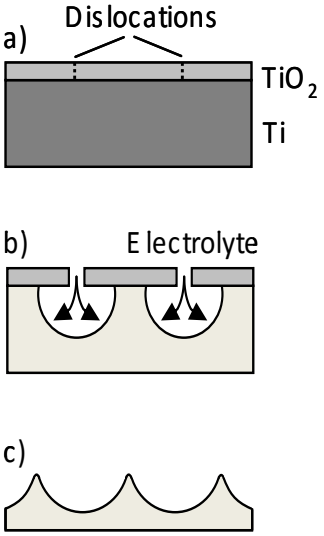


**Fig. 11.** The two-stage process to etch a wave-like surface microstructure.

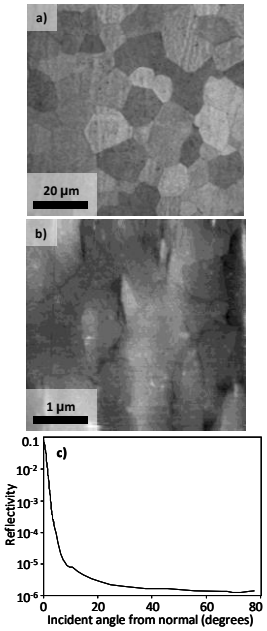


**Fig. 12.** Electropolished (45 V) Ti in the absence of a $TiO_2$ layer: a) microscope image, b) atomic force microscope image, and c) angle-resolved reflectivity.

### *Experimental Results*

In the absence of anodisation, electropolishing provides a smooth clean surface. Optical microscopy shows Ti crystallites ranging in size from 5 µm to 20 µm (figure 12a). Atomic force microscopy provides topographic images from which the surface roughness can be calculated (figure 12b). The rms surface roughness over an area that includes crystallite boundaries is typically 7 nm, while the rms surface roughness within a crystallite is typically 1.5 nm. Angle-resolved reflectivity samples the surface roughness at optical wavelengths over an area of a few millimetres (figure 12c). The slight roughness seen on these scales is caused by uneven mechanical polishing (prior to electrochemical processing) or by slight differences in the angle of crystallite surface facets.

A set of samples were anodized at 20 V and then electropolished at different potentials from 45 V to 75 V for 3 minutes at 40ºC. Electropolishing between 65 V and 75 V reproducibly provided the desired wave-like microstructure (figure 13a).

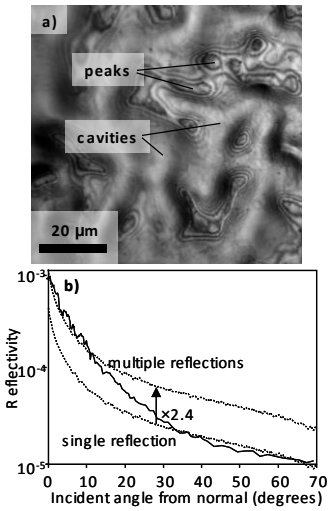


**Figure 13.** a) Optical microscope images showing the desired wave-like microstructure (anodized at 20 V, electropolished at 70 V). b) Experimental (solid) and simulated (dashed) angle-resolved reflectivity.

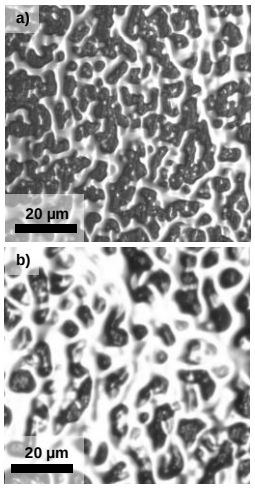


**Fig. 14.** Optical microscope images of samples with incomplete removal of oxide.

## 3. Results and Discussion

The development of the wave-like structure becomes evident from images showing samples where the removal of oxide is incomplete. Examples are provided in figure 4 where the flow rate was insufficient and consequentially the electropolishing rate was reduced. Electropolishing begins at point sites which then elongate and join together to form a network of filaments. Further electropolishing widens and deepens the filaments to create the cavities in the wave-like structure. The surface is clean and has typically 7 nm rms surface roughness on the sub-micron scale. This low surface roughness is critical to avoid short circuits and maintain consistent functionality of subsequent photoactive layers.

## 4. Conclusion

Highly crystalline dispersive NiO nanocrystals have been synthesised with a diameter of 2.5±0.5 nm. It is possible to synthesise nanocrystals without heating which has not been previously reported. Very large rod-shaped particles were selectively synthesised using increased reflux time and reactant concentration,

which can be separated from the smaller particles using filtration or sedimentation. Permittivity and conductivity measurements of nanocrystal solutions provide evidence of rotational and translational degrees of freedom. These initial experiments suggest permittivity measurements are a promising, although non-trivial, method of measuring composition, size, and shape of nanocrystals.

**Acknowledgement**

The authors express their sincere thanks to P.G. Dept. of Applied Physics and Ballistics, FM University, Balasore, India for continuous stimulation and support for the present research.

## REFERENCES

[1] J Houghton, *Global Warming* (Cambridge University Press, 2004).

[2] Renewable Energy Cost of Generation Update, California Energy Commission CEC-500-2009-084 (2009).

[3] MD Archer and AJ Nozik (eds), *Nanostructured and Photoelectrochemical Systems for Solar Photon Conversion* (Imperial College Press, 2007).

[4] AL Rogach (ed), *Semiconductor Nanocrystal Quantum Dots* (Springer Wien New York, 2008).

[5] RD Schaller and VI Klimov, *Phys. Rev. Lett*. **92**, 186601 (2004).

[6] MC Hanna and AJ Nozik, *J. Appl. Phys*. **100**, 074510 (2006).

[7] P Khagram, P Hardy, RMD Brydson, and R Crook, *Proceedings of PVSAT-6, The Solar Energy Society* (Abingdon, UK, 2010).

[8] YL Wu, CS Lim, AIY Tok, HM Lau HM, FYC Boey and XT Zeng, *Nanotechnology* **18**, 215604 (2007).

[9] YL Wu, AIY Tok, FYC Boey and XT Zeng, *2007 IEEE Trans Nanotech* **6**, 497 (2007).

[10] C An, R Wang, S Wang and Y Liu, *Materials Research Bulletin* **43**, 2563-2568 (2008).

[11] Y Li, M Afzaal and P O'Brien, *J. Mater. Chem*. **16**, 2175-2180, (2006).

[12] I Hotový et al, *Journal of Electrical Engineering* **58**, 347-350, (2007).

[13] L Chen, L Li and G Li, *Journal of Solid State Chemistry* **181**, 2073 (2008).

[14] L Chen, L Li and G Li, *Solid State Ionics* **179**, 712-717 (2008).

[15] A Nattestad et al, *Nanotechnology* **19**, 295304 (2008).

[16] Junwu Zhu et al, *Materials Science and Engineering* A **384**, 172 (2004).

[17] J Tauc, *Amorphous and Liquid Semiconductors Plenum* (London, 1974).

[18] P Lommens et al, *Nanotechnology* **19**, 245301 (2008).

[19] KL Lambert et al, *Journal of Colloid and Interface Science* **300**, 597 (2006).

[20] M Poullou, CS Malvi, DW Dixon-Hardy and R Crook, *Scripta Materialia* **62**, 411 (2010).

[21] EW McFarland, *Tang J. Nature* **421**, 616 (2003).

[22] J Tang, H Birkedal, EW McFarland, GD Stucky. *Chem. Commun*. 2278 (2003).

[23] GK Mor, OK Varghese, M Paulose, K Shankar, CA Grimes, *Solar Energy Materials and Solar Cells* **90**, 2011 (2006).

[24] AL Linsebigler, GQ Lu, JT Yates. *Chemical Reviews* **95**, 735 (1995).

[25] D Landolt, *Electrochimica Acta* **32**, 1 (1987).

[26] C Jaeggi, P Kern, J Michler, J Patscheider, J Tharian and F Munnik, *Surf. Interface Anal*. **38**, 182 (2006).

[27] JL Deplancke, A Garnier, Y Massiani and R Winand, *Electrochimica Acta* **39**, 1281 (1994).

[28] J Zhang, K Teng and TJ O'Keefe, *Surface and Coatings Technol*. **89**, 225 (1997).

[29] K Tajima, M Hironaka, K Chen, Y Nagamatsu, H Kakigawa, Y Kozono, *Dental Materials Journal* **27**, 258 (2008).